Magazine of Civil Engineering. 2019. 86(2). Pp. 83–91
Инженерно-строительный журнал. 2019. № 2(86). С. 83–91

Magazine of Civil Engineering

ISSN 2071-0305

journal homepage: http://engstroy.spbstu.ru/

DOI: 10.18720/MCE.86.8

Cracking of tunnel bottom structure influenced by carbonaceous slate stratum

***Y. Zhao*[a*], *Y. Shi*[b], *J. Yang*[a],**
[a] *Central South University, Changsha City, Hunan Province*
[b] *Cccc WuHan Harbour Engineering Design And Research Co.Ltd, Wuhan, China*
** E-mail: zhaoyiding89@126.com*

Keywords: carbonaceous slate; cracking; tunnel bottom structure; numerical analysis.

Abstract. Constructing tunnel is a difficult and expensive process which deserves special attention. In this article, cracking behavior in a highway tunnel structure during construction period is researched, including figuring out the causes and evolution of crack. Large deformation of rock mass is the major inducement of the damaging behavior, which is obtained from the field investigation. The layers of the ground were monitored with the displacement of tunnel while the numerical analysis was realized with extended finite element method. The results highlight the regions of cracking on tunnel bottom structure, which emphasizes the accuracy of model and the influence of poor geological condition. This work demonstrates that the carbonaceous slate stratum plays an important role in the stability of tunnel structure, which leads to the phenomenon of stress concentration in tunnel bottom region. Moreover, the implemented numerical model also simulates the process of the damaging behaviors of tunnel structure induced by the poor geological condition, which is similar to the results from field investigation and provides the design basis for maintenance work.

1. Introduction

Tunnel is an essential and special underground structure in transportation industry such as highway and railway. Complicated geological condition always brings serious challenges to tunnelling work in the mountainous area [1–2], such as landslide, mud gushing, rock burst, collapse of tunnel face and so on. As reported in previously published literatures, these hazards always lead to instability even failure of the tunnel structure. Especially, cracking is a basic form of lining failure [3–6] from construction period to operational period in tunnel, which is usually caused by different causes [7,8] such as geological conditions [9–13], adjacent structure and other natural factor [14–17]. Among them, the large deformation caused by geological condition becomes a hot issue in the construction of mountain tunnel [18, 19]. The large deformation of the surrounding rock is the typical representation in the carbonaceous slate stratum, such as the maximum accumulated settlement of a specific tunnel reaches 1.7 m [20]. Carbonaceous slate has characteristics of low shear strength, joint developed, high sensitivity to vibration, easy to be softened and collapsed [21]. For ensuring the stability and safety of tunnel, field investigation [22–24], numerical simulation [25–28] and model tests [29] are always used to considering the damaging behavior of structure. Nevertheless, few studies focused on the cracking behavior of the tunnel in carbonaceous slate stratum.

Consequently, further study of carbonaceous slate related to damaging behavior is required, which can provide an accurate basis for precaution or maintenance works of the tunnel. In this paper, lining cracking phenomenon of bottom region in a tunnel is presented not only by field investigation and laboratory test but also using numerical analysis, which is aimed at finding out the influence of tunnel structure damaging behaviors due to carbonaceous slate stratum.

Zhao, Y., Shi, Y., Yang, J. Cracking of tunnel bottom structure influenced by carbonaceous slate stratum. Magazine of Civil Engineering. 2019. 86(2). Pp. 83–91. DOI: 10.18720/MCE.86.8.

Джао Я., Ши Я., Янг Д. Растрескивание туннельного днища под влиянием углеродистого сланца // Инженерно-строительный журнал. 2019. № 2(86). С. 83–91. DOI: 10.18720/MCE.86.8

2. Methods

Figure 1 shows the geological condition around the tunnel, in which the longitudinal length is 2262 m and maximum burial depth is 461 m. The stratum around tunnel is comprised of strong or medium weathered carbonaceous slate with thin layer and fracture structure. The integral degree of rock mass is poor and local groundwater is rich, and the surrounding rock is weakened when encountering water and easy to be crushed by hand. Additionally, there is no obvious seismicity around tunnel site.

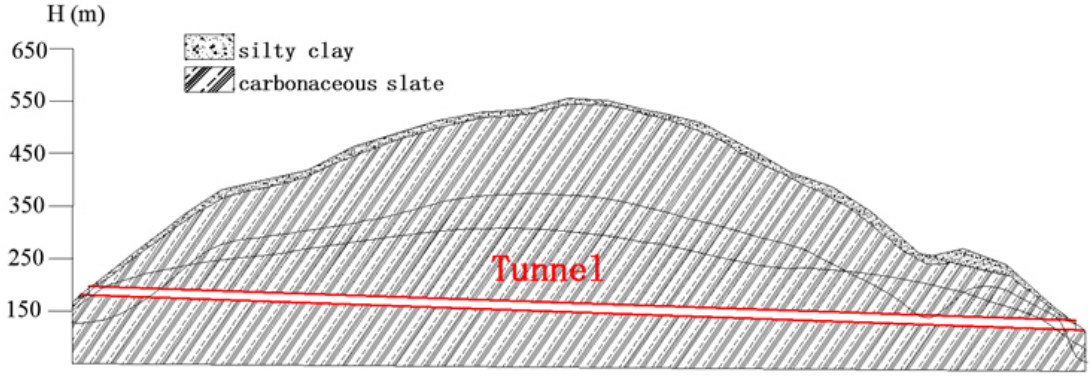

Figure 1. Geological condition of the tunnel.

During the excavation process, it can be observed that exposed surrounding rocks are mainly composed of strongly weathered slate with 0.06–0.2 m thickness. Large deformations of surrounding rock happened frequently during the construction period.

Monitoring displacement of the structure [30] is usually used as an effective method for evaluating construction stability. Figure 2 shows 17-days monitoring results of a cross-section, which includes vertical settlement and horizontal convergence by 5 measuring points as shown in illustrations, which illustrates the total displacements of the shotcrete before supporting secondary lining. The results demonstrate large initial deformation rate, long duration, large deformation and spatial asymmetry of deformation are the deformation characteristics of the tunnel in carbonaceous slate stratum.

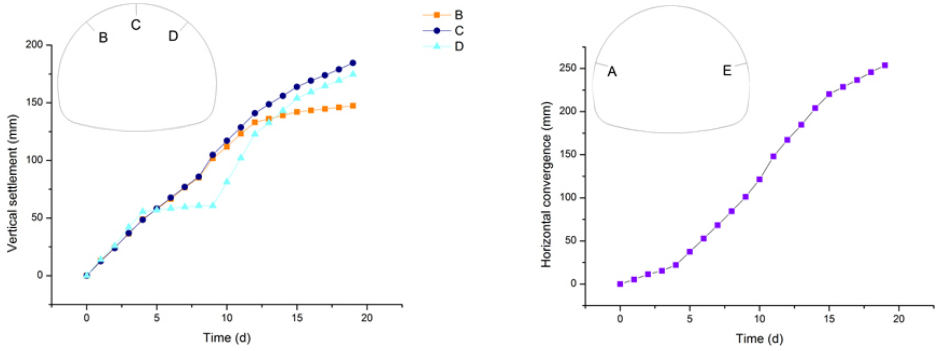

(a) **(b)**

Figure 2. Monitoring results.

A field investigation was implemented according to the large deformation phenomenon, several damaging behaviors were observed during the construction period. The typical damages are shown in Figure 3, which includes: (a) concrete cracking on the ground surface; (b) large deformation of shotcrete; (c) collapse of tunnel surface; (d) cracking of shotcrete; (e) cracking of secondary lining. The aforementioned damaging behaviors have great influences on the schedule, safety and quality of tunnel construction.

Especially, lining cracking was a common phenomenon in this tunnel, which had been already observed in 38.2 % of the construction regions. Figure 4(a) and (b) show two similar cracks at bottom of the tunnel. The burial depths of the cracking regions are almost from 40 m to 50 m, and the cracks at the middle surface of bottom region along with axial direction of the tunnel. The cracks would not only affect the safety of structure but also lead the potential hazard to further traffic. For this reason, the inducement and mechanism of cracks in the bottom region should be analyzed and discussed in this paper.

The surrounding rock (Figure 5) shows typical soft rock properties with characteristic of softening and argillation when contacting water, which might be the cause of large deformation. It is important to figure out the characteristics and compositions of the rock mass, finding out the relationship between carbonaceous slate and large deformation. Thus, X-ray fluorescence spectrum method was used to analyze the material compositions.

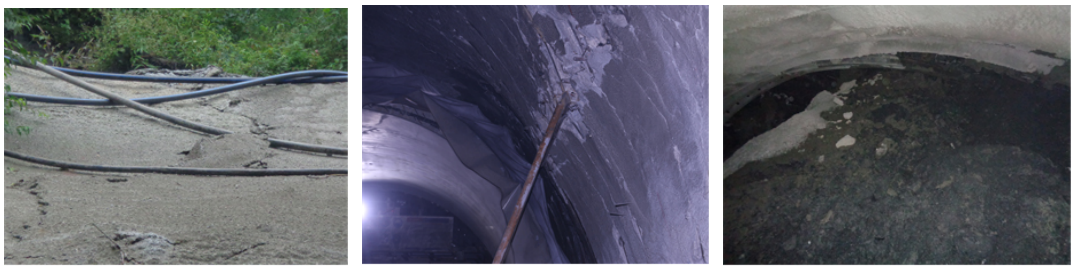

(a) (b) (c)

(d) (e)

Figure 3. Typical damages influenced by large deformation.

(a) (b)

Figure 4. Cracking at the bottom of tunnel.

Figure 5. Surrounding rocks around tunnel face.

It can be obtained from the results of the test report that the surrounding rocks are composed of quartz, muscovite, chlorite, albite, calcite, and dolomite as shown in Figure 6. Among them, the content of quartz, chlorite and white mica accounts for 81.3 % in the whole test block. Clay mineral such as chlorite is easily softened with water, resulting in reduced strength of surrounding rocks over time. The deformation of clinochlore has obvious creep properties [31], and volume will expand by 10 % to 30 %. Additionally, the hydrolysis products of calcite contain kaolin as shown in Equation 1, which is also a clay mineral.

$$4AISi_3O_8 + 6H_2O = AI_4[Si_4O_{10}](OH)_8 + 8SiO_2 + 4H_4SiO_4, \quad (1)$$

where, $AISi_3O_8$ is albite, H_2O is water, $AI_4[Si_4O_{10}](OH)_8$ is kaolin, SiO_2 is quartz and H_4SiO_4 is orthosilicic acid. Calcite and dolomite are the typical carbonate minerals with the capacity of hydrolysis reaction as show in Equation 2, and the surrounding rock with the characteristic of hydrophilic expansion usually contains similar carbonate minerals.

$$CO_3^{2-} + H_2O \leftrightarrow HCO_3^- + OH^-, \quad (2)$$

where, CO_3^{2-} is the carbonate ion, H_2O is water, HCO_3^- is the bicarbonate ions and OH^- is the hydroxyl ion. When the rock is saturated with saturated water, the strength will be reduced. The water will immerse along the joint fractures and weaken the bonding forces between the mineral particles and the rock, for which shear strength and compressive strength are reduced.

Chlorite, albite, calcite, and dolomite account for 37.3 % of the whole test block. Moreover, the degradation, softening, dilatability of these minerals discussed as above should be causes of large deformation. In order to verify the geological condition is the main factor inducing crack, numerical simulation based on ABAQUS [32] is used as an effective method.

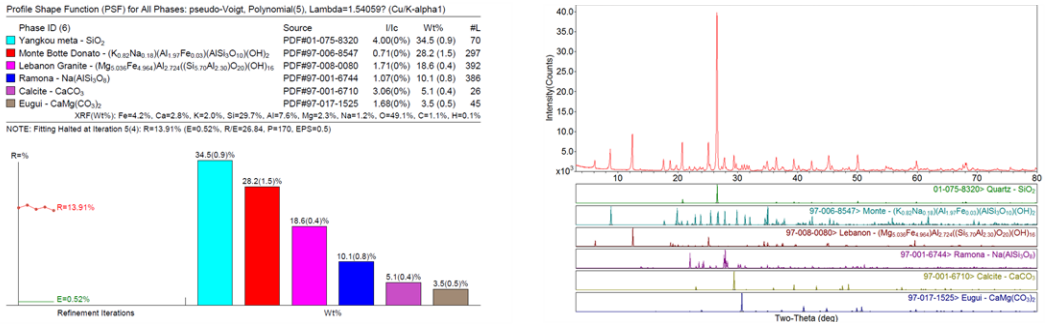

(a) **(b)**

Figure 6. X-ray fluorescence spectrum results.

The qualitative and quantitative analysis of carbonaceous slate can give a reasonable explanation of the rock characteristics around this tunnel. Consequently, the selection of a suitable model for the surrounding rock is the key to establish a reliable numerical model. The rock parameters obtained from geological exploration cannot reflect the realistic characteristics of surrounding rock in the process of simulating, considering of the softening and expansibility of carbonaceous slate. Drucker-Prager yield criterion performances well in simulating the mechanical response of soft rock such as carbonaceous slate [33, 34]. In this work, Drucker-Prager yield criterion is used to reflect carbonaceous slate and the main parameters can be calculated by the following Equations,

$$\beta = \alpha \tan\left(3\sqrt{3}a\right), \tag{3}$$

$$\sigma_c = \frac{3k}{\sqrt{3}-3a}, \tag{4}$$

where β is the internal friction angle in the Drucker-Prager model, σ_c is the calculated uniaxial compression yield stress, α and k should be obtained as follows,

$$\alpha = \frac{\tan(\varphi)}{\sqrt{9+12\tan(\varphi)^2}}, \tag{5}$$

$$k = \frac{3c}{\sqrt{9+12\tan(\varphi)^2}}, \tag{6}$$

where φ is the internal friction angle, c is the cohesive force and these two parameters are selected from the geological exploration report. Especially, associated flow rule is applied in the calculation, which means the dilation angle is equal to β.

After ensuring the reasonability of simulating rock mass, the cracking behavior also needs to be considered. For this reason, the affection of damaging in concrete lining induced by carbonaceous slate must be investigated visually, from which the extended finite element method (XFEM) is adopted in numerical simulation to reflect the crack propagation. XFEM allows local enrichment functions to be easily incorporated into a finite element approximation, which does not require the match of geometry discontinuities and mesh. Therefore, XFEM is a very superduper and effective method to simulate initiation and propagation of a discrete crack along an arbitrary, solution-dependent path without remeshing. The core of XFEM is that it improves the traditional finite element shape function based on the concept of partition of unity method, which is raised by Melenk and Babuska. XFEM allows for the existence of discontinuity in the elements, which can be used to enrich the degree of freedom by special displacement functions.

For the purpose of fracture analysis, the enrichment functions typically consist of the near-tip asymptotic functions that capture the singularity around the crack tip and a discontinuous function that represents the jump in displacement across the crack surfaces as shown in Figure 7 [32]. The approximation for a displacement vector function u with the partition of unity enrichment is

$$u = \sum_{I}^{N} N_I(X)[N_I + H(x)\alpha_I + \sum_{\alpha=1}^{4} F_\alpha(x) b_I^\alpha]. \tag{7}$$

The discontinuous jump function across the crack surfaces, $H(x)$, which is given by

$$H(x) = \begin{cases} 1 & if\,(x-x^*), n \geq 0, \\ -1 & otherwise, \end{cases} \tag{8}$$

where x is a sample (Gauss) point, x^* is the point on the crack closest to x, and n is the unit outward normal to the crack at x^*. $F\alpha(x)$, which are given by

$$F_\alpha(x) = \left[\sqrt{r}\sin\frac{\theta}{2}, \sqrt{r}\cos\frac{\theta}{2}, \sqrt{r}\sin\theta\sin\frac{\theta}{2}, \sqrt{r}\sin\theta\cos\frac{\theta}{2}\right], \quad (9)$$

where (r, θ) is a polar coordinate system with its origin at the crack tip and $\theta = 0$ is tangent to the crack at the tip.

The maximum principal stress criterion can be used to simulate the damaging behavior of secondary lining, which can be represented as,

$$f = \left\{\frac{\langle\sigma_{\max}\rangle}{\sigma^o_{\max}}\right\} \quad (10)$$

Here, $\sigma^o_{\max}$ represents the maximum allowable principal stress. The symbol < > represents the Macaulay bracket with the usual interpretation (i.e., $\langle\sigma_{\max}\rangle = 0$ if $\sigma_{\max} < 0$ and $\langle\sigma_{\max}\rangle = \sigma_{\max}$ if $\sigma_{\max} \geq 0$. The Macaulay brackets are used to signify that a purely compressive stress state does not initiate damage. Damage is assumed to initiate when the maximum principal stress ratio (as defined in the expression above) reaches a value of one.

Once the Drucker-Prager yield criterion and XFEM are confirmed to be used in the numerical model, the simulation process can be advanced. The numerical model and boundary conditions of a typical cross-section are shown in Figure 8, in which the longitudinal calculation range of the numerical model is 112 m, and the vertical calculation ranges of both lateral sides are 50 m, including vertical range of 43 m from tunnel top to the upper boundary. The surrounding rocks and concrete lining in the numerical model are simulated using solid elements in ABAQUS with 2D model considering the stress state of plane strain. Moreover, some assumptions are adopted for the boundary conditions of the numerical model, in which the displacements of the lower boundary are constrained in both longitudinal and vertical directions, those of both lateral boundaries are only restricted in the longitudinal direction, whereas those of upper boundary is free in both longitudinal and vertical directions.

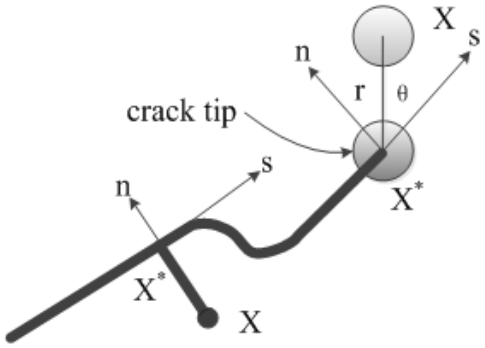

Figure 7. Normal and tangential coordinates of crack.

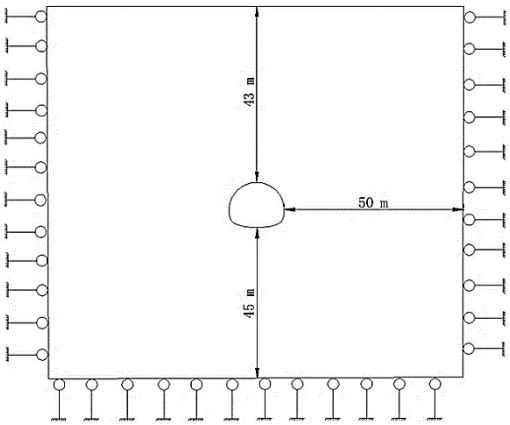

Figure 8. Numerical model and boundary condition.

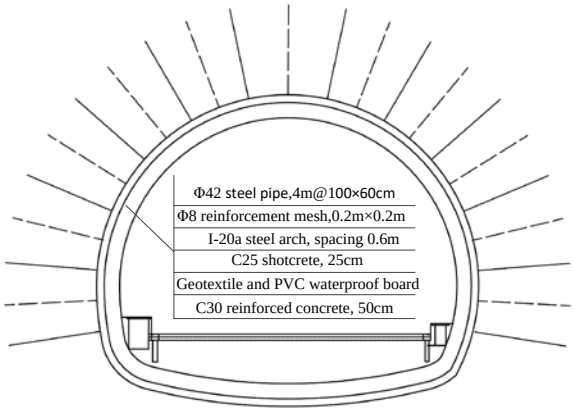

Figure 9. Transverse section of the tunnel structure (unit: m).

In the stage of establishing tunnel structure, Figure 9 shows the typical cross-section of the highway tunnel with 9.2 m height and 12 m width. Shotcrete with 0.25 m thickness and steel mesh with 0.2 m×0.2 m spacing are adopted in the primary lining. For the steel mesh, round bars with 8 mm diameters are both used in longitudinal and circumferential directions. In the anchor system, the 25 mm diameter hollow grouting anchor rod and 22 mm diameter mortar anchor rod with 1 m length and 1.2 m circumferential spacing are respectively fixed at arch part and side wall of surrounding rocks, and 42 mm steel pipes are fixed along longitudinal direction of surrounding rocks before excavating tunnel face. Moreover, the arch vault and side wall as well as inverted arch have 0.5 m thicknesses in the secondary lining.

The secondary lining is considered as ideal elastic material to use XFEM to simulate the process of crack. The damage criterion for traction-separation laws is used for lining damaging evolution, which is according to ultimate tensile strength of concrete with 1.42 MPa. Moreover, the effect of steel arch in primary lining is converted to shotcrete in primary lining by following Equation [35]:

$$E' = E_0 + S_g \cdot E_g / S_c, \tag{11}$$

where E' is equivalent Young's modulus;

E_0 and E_g are Young's modulus of shotcrete and reinforcement respectively;

S_g and S_c are section area of steel arch and shotcrete respectively.

The physical properties of composite lining and surrounding rock are listed in Table 1 as follows. From which, E is elastic modulus, ρ is bulk density, f_c' is compressive strength of concrete, f_t is tension strength of concrete, μ is Poisson's ratio, β is frictional angle (Drucker-Prager yield criterion), k is flow stress ration, φ is dilation angle.

Table 1. Physical properties.

Material	Physical and mechanical parameters
Surrounding rock	E = 800 MPa, ρ = 2200 kg/m^3, μ = 0.32, β = 35º, k = 1, φ = 35°
Primary lining concrete	E = 26 GPa, ρ = 2500 kg/m^3, f_c' = 9 MPa, f_t = 1.0 MPa, μ = 0.23
Secondary lining concrete	E = 31.5 GPa, ρ = 2500 kg/m^3, f_c' = 11 MPa, f_t = 1.42 MPa, μ = 0.2

The cracks were observed several months after finishing the construction of secondary lining, and the tunnel face is almost 80 m away from the cracking region. Thus, full-face excavation of the tunnel is adopted in the simulation process without considering any construction factor [36]. The numerical calculation is implemented as the following stages, 1) establishment of geometric model of stratum and lining systems, adding materials properties and generating mesh; 2) initial step for balance of ground stress; 3) simulation of tunnel excavation and initial support by model change function; 4) Establishment of secondary lining and simulation of the crack influenced by surrounding rock pressure. For simulating the large deformation of rock mass, plane strain elements CPE4R (4-node bilinear, reduced integration with hourglass control) are used in the numerical model.

3. Results and Biscussion

The contour of true strain of lining is shown as Figure 10(b), which demonstrates that the dominant strains are distributed within the tunnel bottom regions. The maximum tensile strains in dominant regions exceed the ultimate value of concrete, which means that lining structure is already damaged at these regions. The results are similar to the illustrated lining failure forms as aforementioned, and which proves the effectiveness of the numerical analysis considering impacts of surrounding rock conditions. Moreover, the evolution of crack can be presented visually through the iso-surface for the signed distance function PHILSM by XFEM, and the outcomes of numerical calculation are shown in Figure 10(a). It can be clearly obtained that there is a tensile type crack generated and cracking is similar to the field conditions, and that confirms the numerical model can simulate the damaging process excellently.

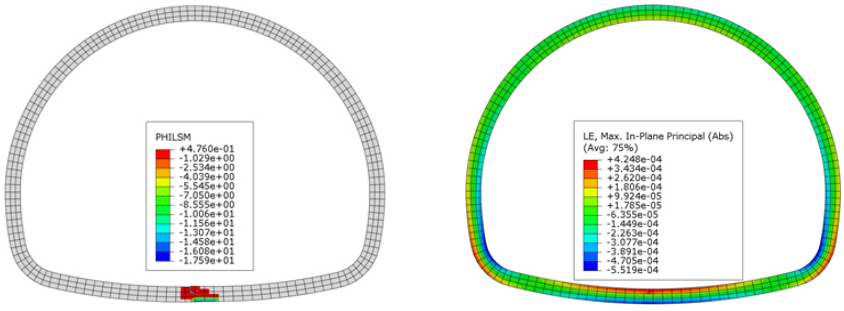

(a) **(b)**

Figure 10. Results of numerical model.

From the partial enlarged view in Figure 11, it can be obtained that the crack generates along the vertical direction on lining surface. The evolution of the force characteristics can be also obtained, in which the traces indicate the movements of bottom structure influenced by the rock mass. Generally, the crack at bottom region is induced by deformation of structure under the tensile stress, which leads to the cracking behaviors and affects the stability of tunnel structure.

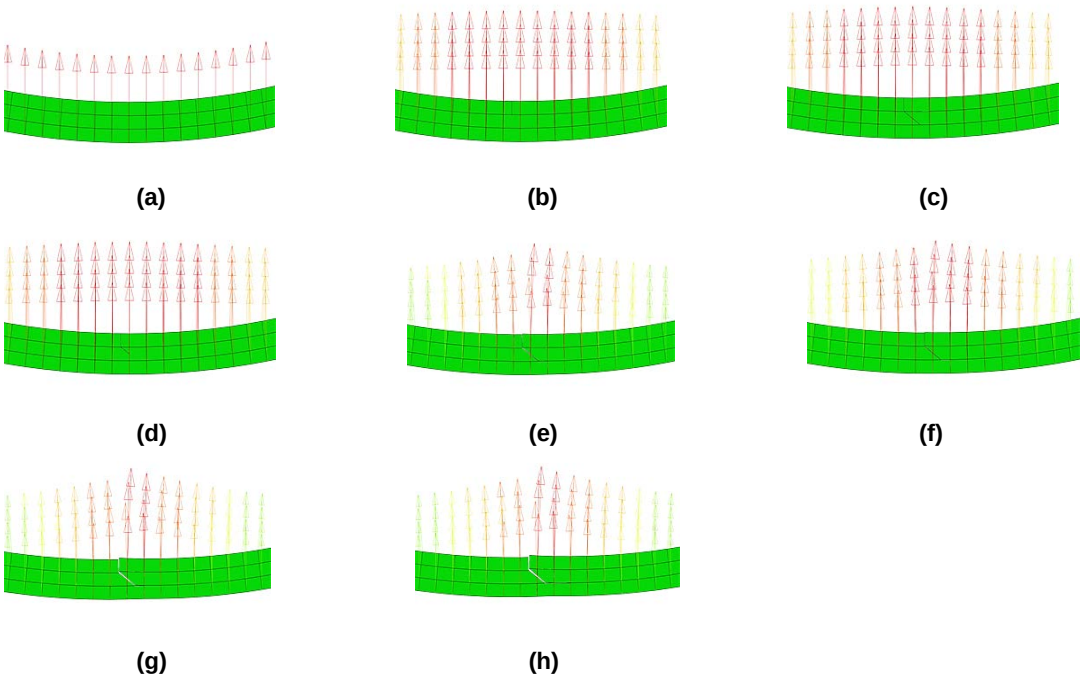

Figure 11. Evolution process of cracking.

Contours of displacements are shown in Figure 12(a) and (b), and the deformation analysis is helpful to confirm the reason for cracking. The results of displacement are similar to the distribution of maximum strain and the maximum total vertical displacement of the tunnel is 0.21 m in the middle region of tunnel bottom, besides, the maximum total horizontal displacement is 0.06 m around two side wall regions. It can be obtained from the numerical results that the geological condition of surrounding rock is the major inducement of cracks in tunnel, which leads to the bottom region becoming the most disadvantaged position of the whole structure. The displacements of the structure verify the reasonability of Drucker-Prager yield criterion for reflecting large deformation of carbonaceous slate. Consequently, strengthening the tunnel structure at bottom region or improving the surrounding rocks conditions are the necessary methods for preventing cracks in subsequent construction or similar engineering projects located in this area.

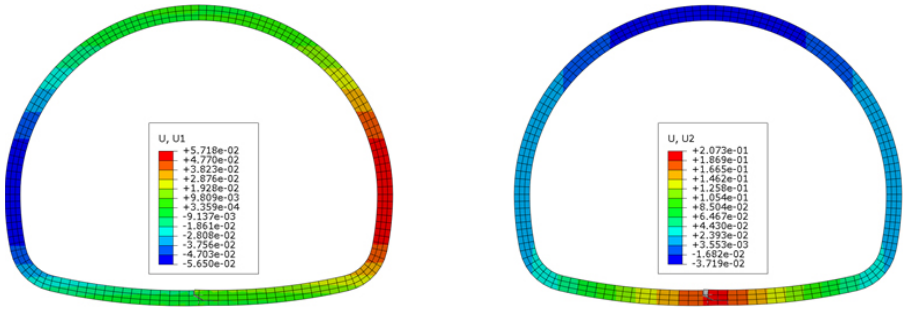

Figure 12. Displacements of tunnel structure.

The outputs of the simulation demonstrate the propagation of the crack and the dangerous region of tunnel. Strengthened design of invert arch, bolting and grouting can be used to avoid the lining cracking of tunnel bottom, and it must be noticed that water should be drained away before the refilling work of inverted arch during the construction period.

4. Conclusion

Field investigation and laboratory test are conducted to identify the inducement of cracks during the construction period. It can be concluded that the geological condition is the major inducement for cracking of tunnel bottom without considering construction factors. In this instance, crack in this tunnel structure is simulated by finite element software to verify if this inducement is reasonable. The following points can be outlined as outcomes of the study,

- Tunnelling in carbonaceous slate stratum may be confronted with difficult construction caused by large deformation of surrounding rock, which has characteristics with high initial deformation rate, long duration, and large deformation. In addition, the large deformation of rock mass will lead to various damaging behaviors, especially cracking of the bottom region.

- The degradation, softening and dilatability of carbonaceous slate influenced by certain minerals should be the direct inducements of the large deformation, which was related to the underground water and inevitable construction water.

- Drucker-Prager yield criterion and XFEM is verified as an effective approach in simulating lining cracking of tunnel bottom in carbonaceous slate stratum. The results show that greater displacement and tensile strain of the bottom region can be obtained than other regions. Moreover, the generation of crack is similar to the realistic damaging behavior in field, which also can verify the cause of crack.

- The contours of total displacement of the secondary lining can also demonstrate that there is an obvious uplift phenomenon of the bottom region, which makes the tunnel bottom become the most disadvantageous part of the whole structure. Thus, necessary measures like strengthened design of tunnel structure need to be implemented in carbonaceous slate stratum. Moreover, water should be drained away before the refilling work of inverted arch.

References

1. Li, S.C., Liu, B., Nie, L.C., Liu, Z.Y, Tian, M.Z., Wang, S.R., Su, M.X., Guo, Q. Detecting and monitoring of water inrush in tunnels and coal mines using direct current resistivity method: a review. Journal of Rock Mechanics and Geotechnical Engineering. 2015. Vol. 7. No. 18. Pp. 469–478.
2. Zhao, Y., Li, P.F., Tian, S.M. Prevention and treatment technologies of railway tunnel water inrush and mud gushing in China. Journal of Rock Mechanics and Geotechnical Engineering. 2013. Vol. 5. No. 6. Pp. 468–477.
3. Federal Highway Administration. Highway and rail transit tunnel inspection manual. 2005. No. 3(4).
4. Sandrone, F., Labiouse, V. Identification and analysis of swiss national road tunnels pathologies. Tunnelling and Underground Space Technology. 2011. Vol. 26. No. 2. Pp. 374–390.
5. Asakura, T., Kojima, Y. Tunnel maintenance in japan. Tunnelling and Underground Space Technology. 2003. Vol. 18. No. 2. Pp. 161–169.
6. Huang, H.W., Liu, D.J., Xue, Y.D., Wang, P.R., Yin, L. Numerical analysis of cracking of tunnel linings based on extended finite element. Chinese Journal of Geotechnical Engineering. 2013. Vol. 35. No. 2. Pp. 266–275.
7. Yamada, T., Sano, N., Baba, K., Yoshitake, I., Nakagawa, K., Nishimura, K. A quantitative criterion for evaluation of tunnel lining concrete. Doboku Gakkai Ronbunshuu F. 2007. Vol. 63. No. 1. Pp. 86–96.
8. Jiang, Y., Tanabashi, Y., Fujii, M., Zhao, X., Idenaga, S. Database development for road tunnel maintenance and management by using geographical information system (new technology for maintenance/retrofit and renewal works in geotechnical engineering: tunnels, underground structures and antiquities). Soil Mechanics and Foundation Engineering. 2004. Vol. 52. Pp. 25–27.
9. Wang, T.T. Characterizing crack patterns on tunnel linings associated with shear deformation induced by instability of neighboring slopes. Engineering Geology. 2010. Vol. 115. No. 1–2. Pp. 80–95.
10. Zhang, Y.X., Shi, Y.F., Zhao, Y.D., Fu, L.L., Yang, J.S. Determining the cause of damages in a multiarch tunnel structure through field investigation and numerical analysis. Journal of Performance of Constructed Facilities. 2017. Vol. 31. No. 3. Pp. 1–7.
11. Lai, H., Song, W., Liu, Y., Chen, R. Influence of flooded loessial overburden on the tunnel lining: case study. Journal of Performance of Constructed Facilities. 2017. Vol. 31. No. 6. Pp. 1–11.
12. He, W., Wu, Z., Kojima, Y., Asakura, T. Failure mechanism of deformed concrete tunnels subject to diagonally concentrated loads. Computer-aided Civil and Infrastructure Engineering. 2009. Vol. 24. No. 6. Pp. 416–431.
13. Bukhartsev, V.N., Volkov, E.N. Influence of discontinuities on the rock mass stress-strain state around excavation. Magazine of Civil Engineering. 2013. 39(4). Pp. 3–11. DOI: 10.5862/MCE.39.1
14. Roy, N., Sarkar, R. A review of seismic damage of mountain tunnels and probable failure mechanisms. Geotechnical and Geological Engineering. 2017. Vol. 35. No. 1. Pp. 1–28.
15. Mohamad, H., Bennett, P.J., Soga, K., Mair, R.J., Bowers, K. Behaviour of an old masonry tunnel due to tunnelling-induced ground settlement. Géotechnique. 2015. Vol. 60. No. 12. Pp. 927–938.
16. Bian, K., Liu, J., Xiao, M., Liu, Z. Cause investigation and verification of lining cracking of bifurcation tunnel at Huizhou Pumped Storage Power Station. Tunnelling and Underground Space Technology. 2016. Vol. 54, No. 27, Pp. 123–134.
17. Tan, Y., Smith, J.V., Li, C.Q., Currell, M., Wu, Y. Predicting external water pressure and cracking of a tunnel lining by measuring water inflow rate. Tunnelling and Underground Space Technology. 2018. Vol. 71. Pp. 115–125.
18. Wang, B., Li, T.B., He, C., Zhou, Y. Analysis of failure properties and formatting mechanism of soft rock tunnel in meizoseismal areas. Chinese Journal of Rock Mechanics and Engineering. 2012. Vol. 31. No. 5. Pp. 928–936.
19. Lei, J., Zhang, J.Z., Lin, C.N. Analysis of stress and deformation site-monitoring infault zone of Wushaoling tunnel under complex geological conditions. Rock and Soil Mechanics. 2008. Vol. 29. No. 5. Pp. 1367–1371.
20. Wu, J.G., Liu, X.X., Wang, W.X. Deformation control technology during the construction of large section carbonaceous slate formation tunnel. Modern Tunnelling Technology. 2011. Vol. 46. No. 2. Pp. 68–72.
21. Wang, W.L., Wang, T.T., Su, J.J., Lin, C.H., Seng, C.R., Huang, T.H. Assessment of damage in mountain tunnels due to the taiwan chi-chi earthquake. Tunnelling and Underground Space Technology. 2001. Vol. 16. No. 3. Pp. 133–150.
22. Kontogianni, V.A., Stiros, S.C. Induced deformation during tunnel excavation: evidence from geodetic monitoring. Engineering Geology. 2005. Vol. 79. No. 1–2. Pp. 115–126.

23. Lai, J., Fan, H., Chen, J., Qiu, J.X., Wang, K. Blasting vibration monitoring of undercrossing railway tunnel using wireless sensor network. International Journal of Distributed Sensor Networks. 2015. No. 6. Pp. 1–7.
24. Gao, Y., Xu, F., Zhang, Q., He, P., Qin, Z. Geotechnical monitoring and analyses on the stability and health of a large cross-section railway tunnel constructed in a seismic area. Measurement. 2018. No. 122. Pp. 620–629.
25. Zhao, Y.D., Shi, Y., Yang, J.S. Study of the influence of train vibration loading on adjacent damaged tunnel. Shock and Vibration. 2019. Vol. 2019. Pp. 1–8.
26. Geniş, M. Assessment of the dynamic stability of the portals of the Dorukhan tunnelusing numerical analysis. International Journal of Rock Mechanics and Mining Sciences. 2011. Vol. 47. No. 8. Pp. 1231–1241.
27. Fang, Y., Xu, C., Cui, G., Kenneally, B. Scale model test of highway tunnel construction underlying mined-out thin coal seam. Tunnelling and Underground Space Technology. 2016. Vol. 56. Pp. 105–116.
28. Ivanes, T.V., Kavkazskiy, V.N., Shidakov, M.I. Geomechanical tasks solving in modelling of temporary support parameters in Sochi tunnels. Procedia Engineering. 2017. Vol. 189. Pp. 227–231.
29. Idinger, G., Aklik, P., Wu, W., Borja, R.I. Centrifuge model test on the face stability of shallow tunnel. Acta Geotechnica. 2011. Vol. 6. No. 2. Pp. 105–117.
30. Benin, A., Konkov, A., Kavkazskiy, V., Novikov, A., Vatin, N. Evaluation of deformations of foundation pit structures and surrounding buildings during the construction of the second scene of the state academic mariinsky theatre in saint-petersburg considering stage-by-stage nature of construction process. Procedia Engineering. 2016. Vol. 165. Pp. 1483–1489.
31. Yu, D.H., Peng, J.B. Experimental study of mechanical properties of chlorite schist with water under triaxial compression. Chinese Journal of Rock Mechanics and Engineering. 2009. Vol. 28. No. 1. Pp. 205–211.
32. Dassault Simulia International Inc. ABAQUS v 6.4. 2004.
33. Wang, W.M., Zhao, Z.H., Wang, L. Safety analysis for soft rock tunnel floor destruction based on different yield criterions. Chinese Journal of Rock Mechanics and Engineering. 2012, Vol. 31. No. S2. Pp. 3920–3927.
34. Deng, C.J., He, G.J., Zheng, Y.R. Studies on Drucker-Prager yield criterions based on M-C yield criterion and application in geotechnical engineering. Chinese Journal of Geotechnical Engineering. 2006. Vol. 28. No. 6. Pp.735–739.
35. Zhao, Y.D., Liu, C., Zhang, Y.X., Yang, J.S., Feng, T.G. Damaging behavior investigation of an operational tunnel structure. Engineering Failure Analysis. 2019. No. 47. Pp. 25–33.
36. Abdullayev, G.I., Velichkin, V.Z., Soldatenko, T.N. The organizational and technological reliability improvement in construction by using failure prediction method. Magazine of Civil Engineering. 2013. 38(3). Pp. 43–50. DOI: 10.5862/MCE.38.6

Contacts:

Yiding Zhao, +008618118686057; zhaoyiding89@126.com
Yao Shi, +008615861927700; 734169065@qq.com
Junsheng Yang, +8618075154205; 1797935162@qq.com